www.czasopisma.pan.pl PAN POLSKA AKADEMIA NAUK www.journals.pan.pl

Arch. Metall. Mater. **70** (2025), 4, 1685-1692

DOI: https://doi.org/10.24425/amm.2025.156249

MANOJ KUMAR ELIPEY[1], P.S. KISHORE[1*], B. RATNA SUNIL[2]

MECHANICAL PROPERTIES AND MACHINING BEHAVIOR OF AZ31-CALCIUM DEFICIENT HYDROXYAPATITE (CDHA) BIODEGRADABLE COMPOSITES

In order to create biodegradable magnesium-based implants, calcium-deficient hydroxyapatite (CDHA) nanoparticles were incorporated into AZ31 magnesium (Mg) alloy using friction stir processing. When compared to the AZ31 base alloy (41.4±5.9 µm), the composites showed grain refinement up to 1.8±1.9 µm. The composition of the produced composites is confirmed by characterization using electron microscopy and X-ray diffraction analysis. Because of the reduced grain size and the added nano-CDHA, the composite's hardness (91±12.6 HV0.1) was higher than the parent alloy's (46±3.3 HV0.1). Both the base alloy and the composite have undergone uni-axial tensile testing. In comparison to the basic alloy (225±4.9 MPa), the grain refined composite has demonstrated a comparatively higher strength (283.6±5.1 MPa). Machining studies carried out by drilling experiments at 90 rpm and 180 rpm with 15 mm/min and 30 mm/min feed revealed higher cutting forces for the composites. However, the edge damage in the produced holes was observed as significantly lower for the composites compared with the base alloy.

Keywords: AZ31 magnesium alloy; CDHA; hydroxyapatite; degradable implant; tensile strength; drilling

1. Introduction

By choosing the right fractions of the constituent phases, composite materials can be manufactured to have hybrid qualities [1]. The scientific literature has recently seen a huge increase in research on creating magnesium (Mg)-based composites for use in bone implants [2, 3]. The primary goals of creating a variety of biocompatible Mg composites are to improve tissue-implant interactions and control deterioration [4,5]. In the development of Mg composites for biomedical applications, a number of dispersion phases, including hydroxyapatite, tricalcium phosphate, Al_2O_3, TiO_2, and carbon nanotubes (CNTs), are frequently employed as reinforcing phases [4]. Important Mg-based composites made for biomedical applications include Mg-HA [6,7], Mg-β-TCP [8], Mg-HA/MgO [9], AZ31-CNT [10], Mg-1Sn-Al_2O_3 [11], ZK60A-calcium phosphate [12], AZ91-HA [13], AZ91-FA [14], $Mg_{66}Zn_{30}Ca_4$-BMG [15], Mg-Ca-HA/TCP [16], Mg_2Zn-Al_2O_3 [17], ZK60-HA [18], and Mg-TiO_2 [19]. Since calcium (Ca) – based mineral phases make up natural bone, they were given precedence over other ceramic phases. In order to create degradable Mg composites, hydroxyapatite (HA), a calcium phosphate (Ca/P) phase that is a member of the apatite family and has exceptional bioactivity, has emerged as the preferred dispersion phase [19, 20]. By using micro-level HA as the dispersion phase, Ikuho Nakahata et al. [6] were able to increase the Mg-HA composite's corrosion resistance and mechanical performance. A number of documented techniques, such as powder metallurgy, casting, hot extrusion, laser melting, and friction stir processing (FSP), can be used to add HA to Mg matrix [4-6].

One of the most effective ways to enhance the performance of Mg implants in the bioenvironment is to refine their microstructure. A number of recent investigations have documented improved performance of Mg alloys intended for medical applications following grain refining [21-29]. Among the available mechanical processes to induce grain refinement in Mg alloys, FSP offers several benefits. Grain refined structures with comparatively lower defects are produced using FSP [32]. In addition to the advantages of grain refinement, FSP can be used to reinforce secondary phases into metallic sheets and plates to create composites, which combine the advantages of dispersed phases and refined microstructure [33]. The produced composites exhibits the presence of incorporated secondary phases at the surface and also at the cross section of the processed zone up to a thickness

[1] ANDHRA UNIVERSITY, DEPARTMENT OF MECHANICAL ENGINEERING, COLLEGE OF ENGINEERING (A), VISAKHAPATNAM, ANDHRA PRADESH, INDIA
[2] PRINCE MOHAMMAD BIN FAHD UNIVERSITY, DEPARTMENT OF MECHANICAL ENGINEERING, COLLEGE OF ENGINEERING, AL-KHOBAR 31952, SAUDI ARABIA
* Corresponding author: prof.pskishore@andhrauniversity.edu.in

equals to that of tool pin length. When HA was included by FSP using various Mg alloys as matrix materials, the resulting composites showed good bioactivity and controlled degradation [6,34-36]. HA is a Ca and P ceramic phase that exhibits a Ca/P ratio of 1.67 [37,38]. In contrast to stable HA, a ceramic phase known as calcium deficient HA (CDHA) has a degradable nature in the bioenvironment if the Ca/P ratio is less than 1.67 [38,39]. Hence, CDHA is used in biodegradable applications in developing degradable bone filling materials and in local drug delivery applications. Both Mg and CDHA are degradable in nature, compared with stable HA. Furthermore, compared with Mg, the degradation rate of CDHA is relatively slow and it stays for longer time and favours the bone remodelling during the healing process. After the fractured bone is completely healed, the presence of any implant material is not required. Since CDHA is bioactive material which promotes osseointegration and also a degradable material which does not stay for longer time, dispersing CDHA in Mg to develop degradable composite is an optimum choice. There is not enough information in the literature on producing Mg based composites with CDHA reinforcement. Our first research revealed that the FSP-developed AZ31-CDHA composite has outstanding corrosion resistance [40].

Since, the developed Mg composite need to be subjected to machining to manufacture desired components, understanding the machining characteristics of these grain refined composites is essential. Surya Kiran et al. [41] showed that the FSPed AZ91 Mg alloy resulted in higher cutting forces due to fine grains and solid solution strengthening. Additionally, Hemendra et al. [42] used three distinct pin profiles to do FSP of AZ91 Mg alloy, and they found that the machinability was affected by the reduction in grain size brought on by FSP. Venkataiah et al [43] also produced grain refined ZE41 Mg alloy by FSP and from the machining studies, improved machining characteristics were observed due to the decreased intermetallic fraction and smaller grain size after FSP. However, information on machining studies on grain refined biodegradable AZ31 composites is lacking in the literature. Hence, the present work aims to develop AZ31-nano-CDHA composite by FSP with an objective to study the role of microstructure and presence of CDHA on mechanical properties and machining behaviour by conducting drilling experiments.

2. Materials and methods

The commercially available AZ31 Mg alloy rolled sheets (6 mm thick) having chemical composition of 2.9% Al, 1.05% Zn, 0.2% Mn, with the rest being Mg by weight, were procured from Exclusive Magnesium, India. 100 mm × 50 mm × 6 mm samples were cut, and the workpiece surface to be filled with nano-CDHA was machined with holes that were 1 mm in diameter and 2 mm deep, as shown schematically in Fig. 1(a). Nano-CDHA was synthesized using chemical precursors according to the reported procedure [38,39]. The CDHA powders were characterized by Transmission electron microscopy (HRTEM, Philips, Holland) and X-ray diffraction (XRD, Bruker, USA). Initially, a pin-less FSP tool was used to seal the surface holes to stop the filled powders from escaping during the process. The workpiece surface was then subjected to friction stir processing to produce the composite. Based on previously published research, the processing parameters (1400 rpm speed and 25 mm/min feed) were selected [35,44]. The FSP tool with a threaded tapered pin profile was utilized in this work since it produces a greater amount of material flow in the stir zone [32]. The FSP tool pin dimensions used in this work are shown in Fig. 1(b).

After metallographic polishing, picric acid etchant (100 g of picric acid, 5 ml of distilled water, 5 ml of acetic acid and 5 ml of ethanol) was used to etch the basic material and the produced composites. The samples were analyzed using an optical microscope (Olympus BX63, Germany) and a scanning electron microscope (SEM, TESCAN, Czech Republic). Area EDS analysis was carried out to assess the chemical composition of the samples. The linear intercept method was used to determine the average grain size from the recorded microstructures [45]. Optical micrographs (collected at 3 different locations) obtained at 200× magnification were used to measure the average grain size. During the measurements, intermetallic particles were

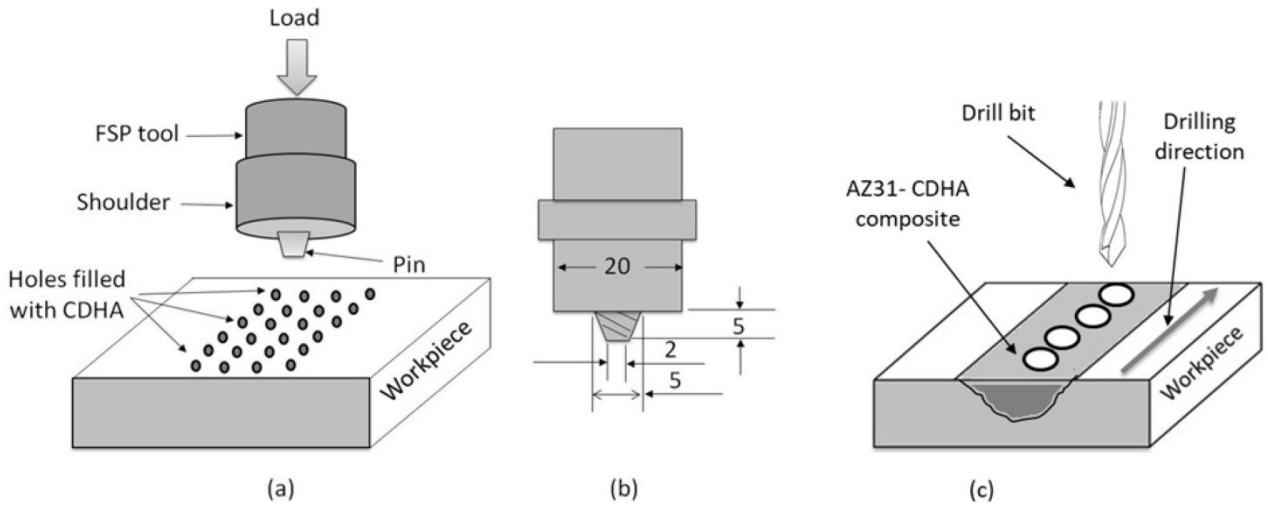

Fig. 1. Schematic representation of (a) FSP, (b) tool dimensions and (c) drilling experiments

omitted in both the base alloy and the composite. XRD analysis (D8, Bruker, USA) was performed on both the base alloy and the composite.

Specimens were cut from the center of the FSPed region for hardness measurements and tensile tests. Tensile samples were prepared such that the FSPed region comes in the gauge length of the samples. Vicker's indentation method was used to measure the microhardness of the base material and the generated composite at the cross section by applying a 100 g force for 15 s. Three measurements on average were taken across the generated composite at intervals of one mm. Tensile experiments were carried out by preparing sub-size tensile specimens as per ASTM E8 standards [46]. Tensile experiments were conducted by applying 0.01/s strain rate by using a universal testing machine (Carl-Zwick, Germany). Drilling experiments were conducted to evaluate the machining behaviour of the produced composites. The samples were placed on a dynamometer platform (Kistler, Switzerland) that was attached to a vertical milling machine work table. The drilling experiments were then carried out using a 6 mm diameter twist drill bit to produce holes at spindle speeds of 90 and 180 rpm at feed rates of 15 mm/min and 30 mm/min without using any coolant. From the recorded cutting forces, mean cutting force values were obtained. The drilling experiments were conducted on the FSPed surface of the composite along the FSP direction in the center of the stir zone as shown in Fig. 1(c). The thickness of modified surface is around 5 mm as the tool pin length is 5 mm. The diameter of the drill bit is 6 mm which produces holes of 6 mm diameter. Drilling was carried out for few seconds till the cutting forces were stabilized. The resulting holes were observed with around 3-4 mm depth. Therefore, it is confirmed that the drilling occurs within the processed zone.

3. Results and discussion

In order to produce the composite, reinforcements were inserted into the surface holes and stirred by the FSP non-consumable tool [32,33]. Fig. 2(a) displays the nano-CDHA

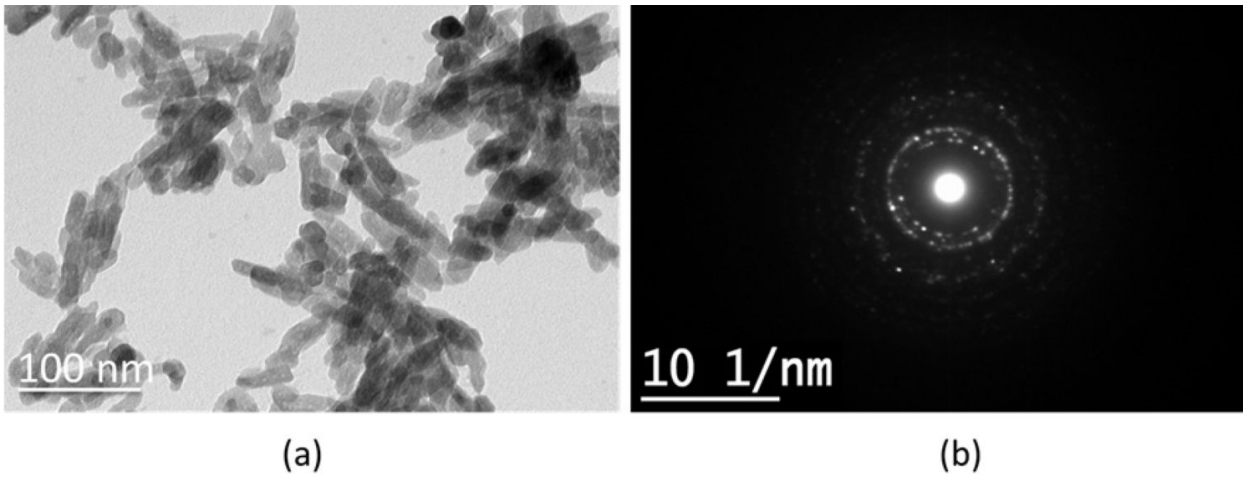

Fig. 2. (a) bright field TEM image of nano-CDHA and (b) corresponding electron diffraction pattern

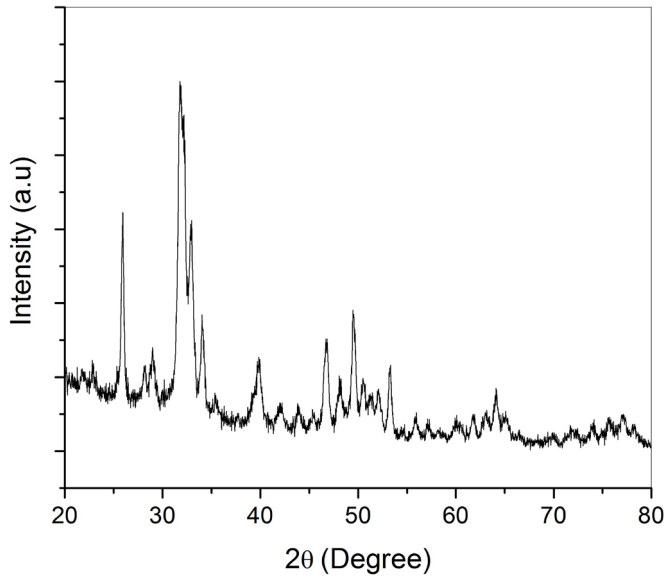

Fig. 3. XRD pattern of nano-CDHA

crystals as observed form TEM, from which the crystallite size was determined as less than 50 nm. The bright spots in the electron diffraction pattern (Fig. 2(b)) showed up as a ring pattern, indicating that the CDHA crystals were nanoscale. Fig. 3 shows the XRD pattern of nano-CDHA used in the present work. All the peaks were identified and indexed. No impurities were observed in the prepared nano-CDHA.

The SEM image of AZ31 alloy is shown in Fig. 4(a) and the corresponding EDS is shown in Fig. 4(b). At the room temperature, formation of $Mg_{17}Al_{12}$ intermetallic is typically observed near the grain boundaries of the alloy because of the reduced solubility (<1%) of Al in Mg. In addition to intermetallic areas, the AZ31 alloy microstructure displays a mixture of solid solution grains made from Mg and Al. From the SEM microstructure, it is clearly observed the solid solution grains and the intermetallic network. Presence of Mg, O, Al and Zn from the EDS analysis confirm the base alloy chemical composition.

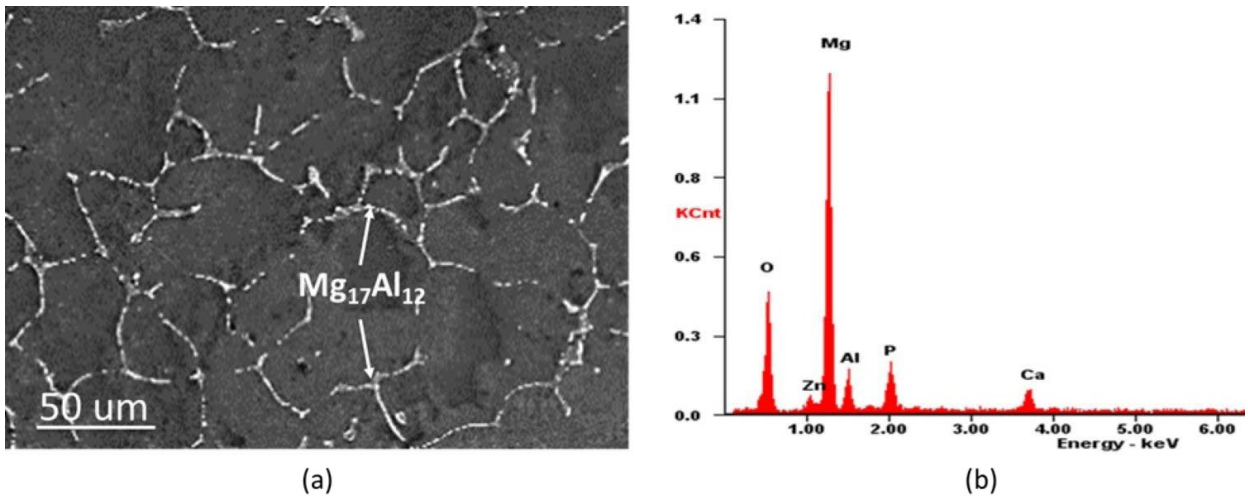

Fig. 4. (a) SEM image of AZ31 Mg alloy and (b) corresponding EDS analysis

Presence of peaks corresponding to CDHA and a clear increment in the intensities of (002) and (103) peaks and decrement of intensity of (101) and (200) peaks can be clearly observed in the XRD of the composite (Fig. 5). All the peaks in the XRD of AZ31 were identified as belonging to the α-Mg phase. However, due to the presence of lower amount of intermetallic, the corresponding XRD peaks were not appeared. It is understood from the literature that FSP significantly changes the texture of metals [32]. In the current work, the composite has exhibited preferred orientation dominated by basal texture. This is similar to the other FSPed alloys which also exhibited preferred orientation due to the material flow during plastic deformation [31,35,36]. Since the (002) plane is a high-density plane, the formation of a basal (002) dominated texture aids in altering the bulk properties of the composite in addition to microstructure modification and integrated nano-CDHA.

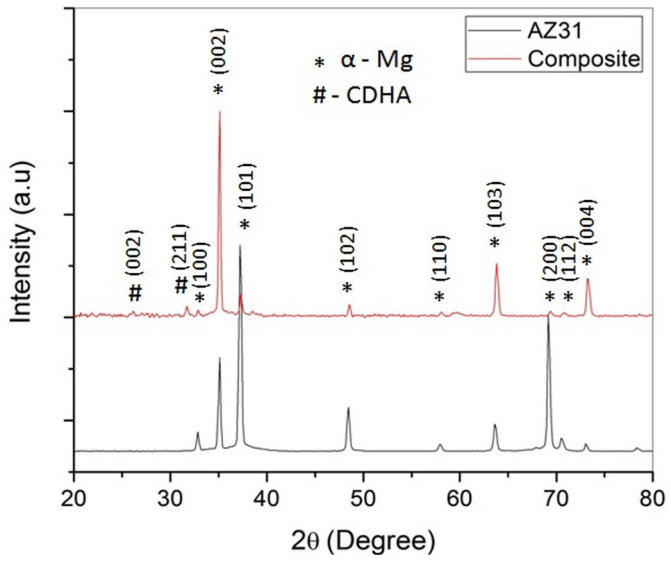

Fig. 5. XRD patterns of the base alloy and the composites

From the microstructural studies (Fig. 6), the produced composite was characterized with fine grains. The agglomerated nano-CDHA was observed in the composite (Fig. 6(a)), and the corresponding EDS analysis (Fig. 6(b)) confirms the presence of Ca and P in addition to Mg, O, Al and Zn. Compared with the average grain size (41.4±5.9 μm) of the base alloy (Fig. 4(a)), significant grain size reduction up to 1.8±1.9 μm was observed in the composite (Fig. 6(c)). Grain refinement in FSP is typically caused by dynamic recrystallisation, which can be attributed to the microstructure refinement in the composite. Grain refining is aided by the presence of nano-CDHA crystal, which inhibits grain growth. Grain refinement is an advantage of using FSP to produce composites compared with the melting and solidification methods.

The average microhardness of the samples is compared in Fig. 7(a). Significant improvement in the measured hardness was oberved in the composites due to the smaller grain size and the incorporated nano-CDHA. Fig. 7(b) presents the yield strength and ultimate tensile stregth (UTS) of the samples. The improvement in the strength of the composite compared with the base alloy is significant which is claimed to grain boundary strengthening and the dispesion strengthening mechanisms. However from the observed tensile test data, the persentage of elongaiton values of the samples were observed as similar; i.e. 9.73±1.7 and 8.2±1.5 for AZ31 and the composite respectively. From the results, it is understood that the strength of the composite was increased and the change in % of elongation is insignificant.

Fig. 8 shows typical cutting force profiles of the AZ31 alloy and the composites machined at 15 mm/min feed at two different speeds 90 rpm and 180 rpm. The mean cutting forces of the samples observed at the stabilized cutting force profile at all the cutting parameters are compared in Fig. 9. It is evident that with the increased cutting speed from 90 rpm to 180 rpm, cutting force was decreased in both the samples at both the feed rates. This is due to the generation of heat with the increased cutting speed which decreases the resistance force of the sample during drilling. Compared with the base alloy, composite exhibited higher cutting forces at all the cutting parameters due to the increased hardness and mechanical strength in addition to the presece of nano-CDHA in the composite. However, the edges of the produced holes were observed with lower level of material

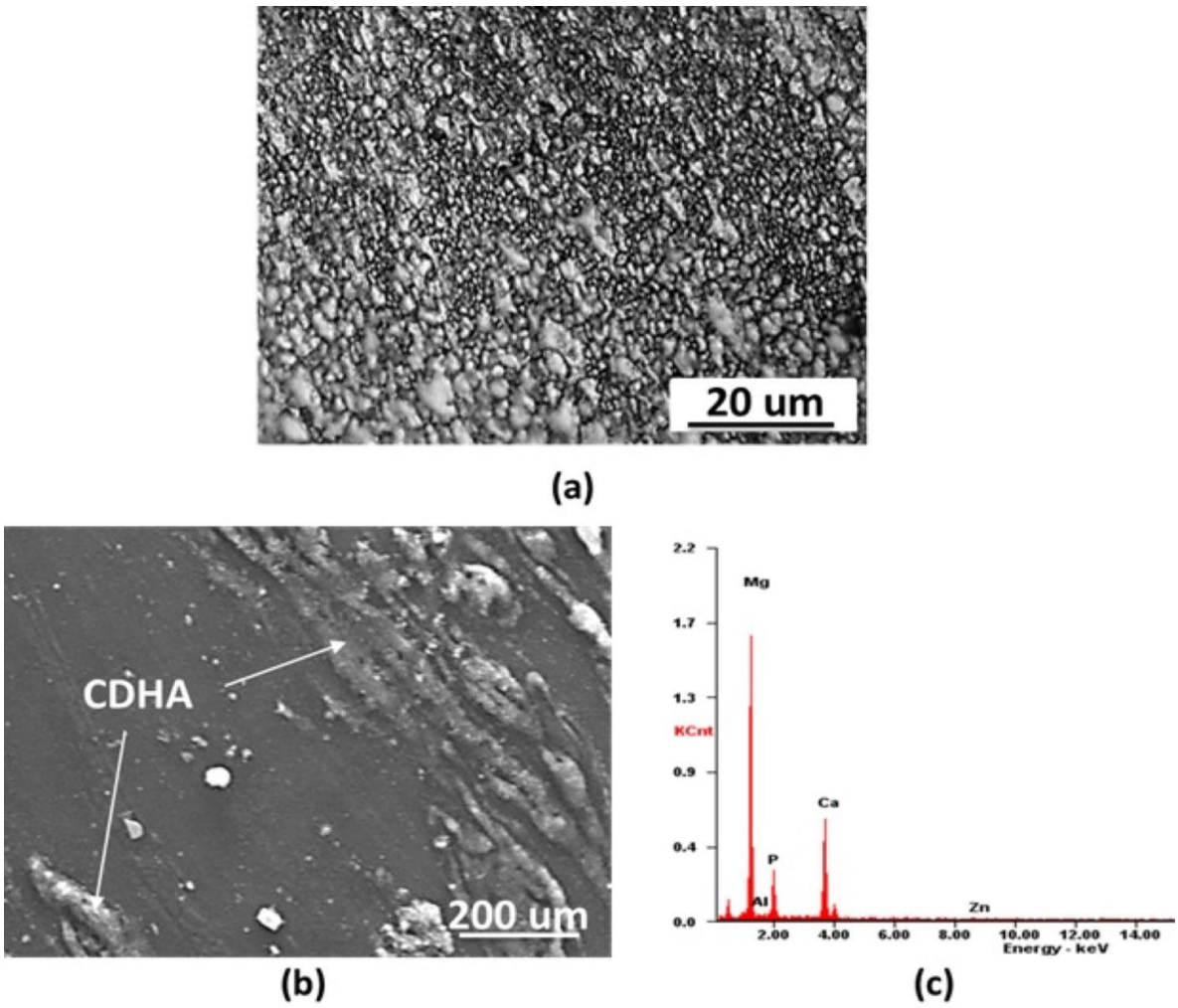

Fig. 6. Microstructural observations of the composite: (a) optical microscope image (b) SEM image (SE mode) and (c) corresponding area EDS analysis

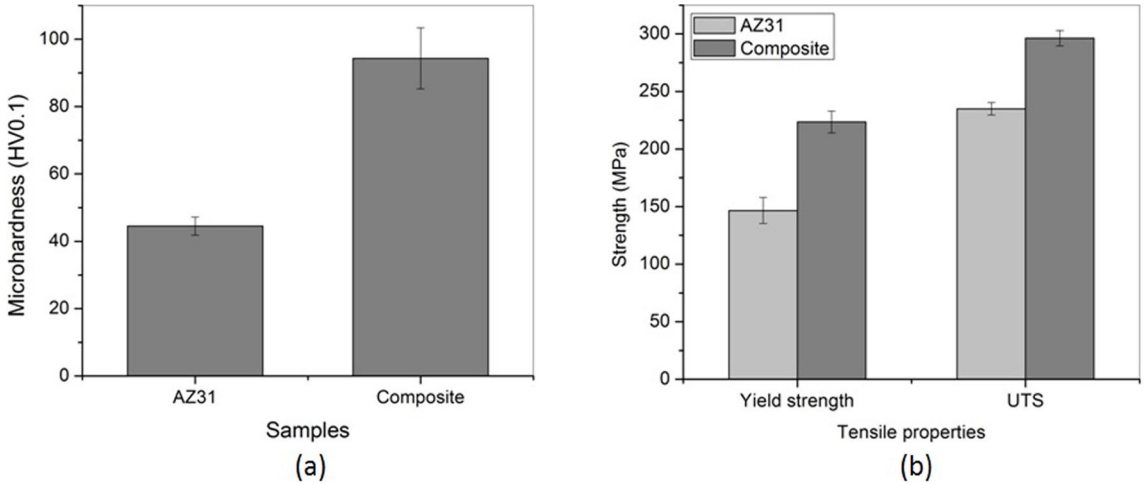

Fig. 7. Mechanical properties of the samples: (a) microhardness measured from Vickers indentation method and (b) tensile properties obtained from the uniaxial tensile tests

delamination in the composites compared with the base alloy. This is due to the grain refinement and the reduced intermetallic as also observed in AZ91 and ZE41 Mg alloys as reported in the earlier works [41-43].

The findings show that FSP can be used to produce AZ31-CDHA composites with reduced grain size and basal-dominated texture. Furthermore, better mechanical performance as reflected from the increased hardness and strength also can be achieved

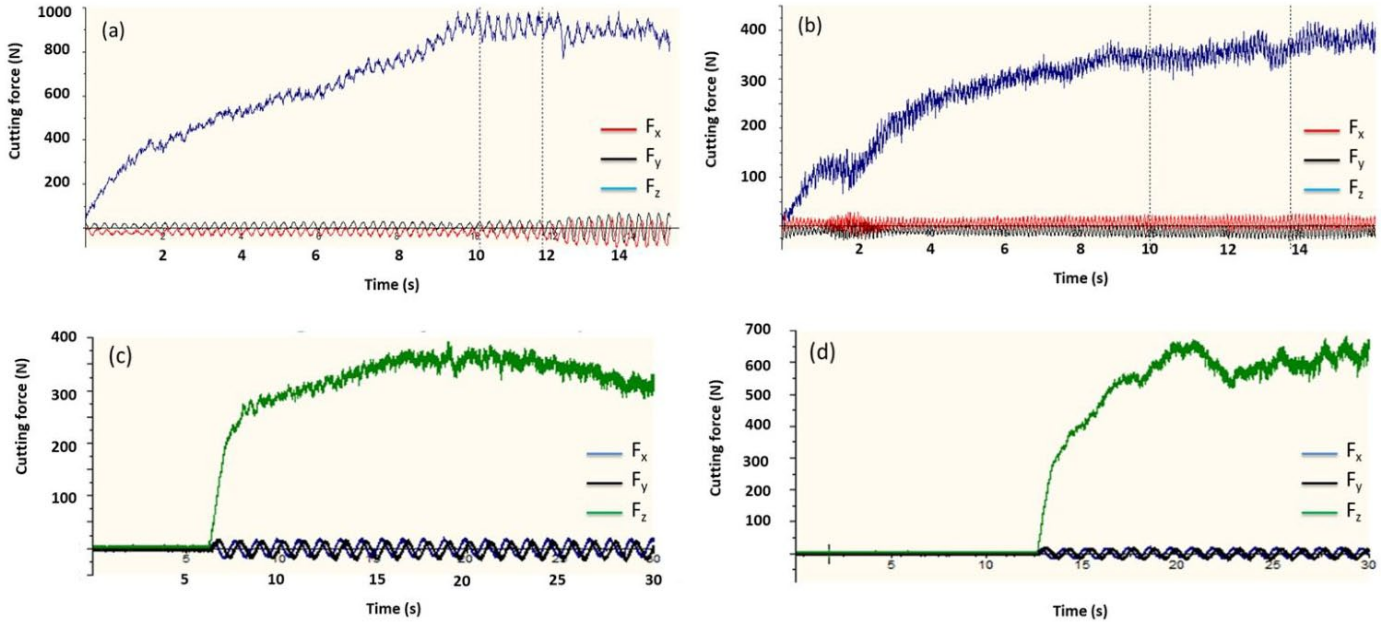

Fig. 8. Typical cutting force (Fz) profiles of the samples machined at 15 mm/min feed: (a) composite at 90 rpm, (b) composite at 180 rpm, (c) AZ31 at 90 rpm and (d) AZ31 at 180 rpm

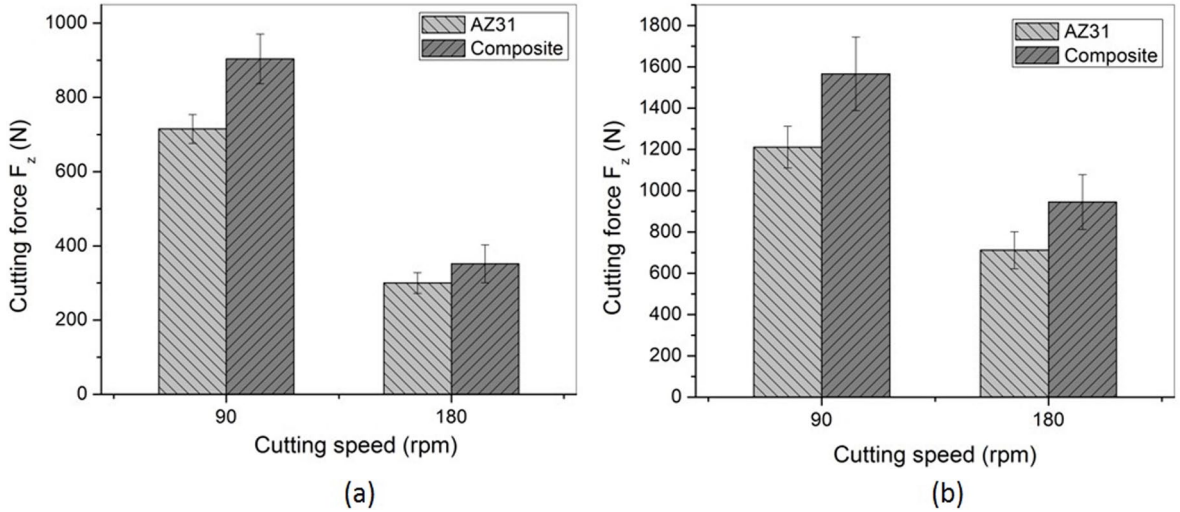

Fig. 9. comparison of the mean cutting forces of the samples: (a) 15 mm/min feed and (b) 30 mm/min feed

in AZ31-nano-CDHA composite. From the machining studies by conducting drilling experiments, in spite of increased cutting forces, lower damage was observed for the produced holes. In order to produce Mg based composites, HA (with a Ca/P stochastic ratio of 1.67) has been widely used as the dispersion phase in a few reports [5]. However, compared to HA, nano-CDHA can dissolve more quickly, and the implant composed of nano-CDHA does not leave any residues at the interface between the implant and bone. Therefore, selecting degradable nano-CDHA as dispersing phase to produce Mg based degradable implants is more viable for temporary orthopedic applications. The current study also demonstrates the feasibility of machining operations to manufacture medical implants by using AZ31-nan-CDHA composites. It is summarized from the current study that the grain refinement by FSP and incorporating nano-CDHA in the composite enhances the mechanical performance of the composite and marginally increases the difficulty in machining during drilling with superior finishing.

4. Conclusions

In the present work, friction stir processing (FSP) was used to produce composites of AZ31 Mg alloy – nano-calcium deficient hydroxyapatite (CDHA) composite for degradable bone implants application. From the results, the following conclusions are drawn.

i. FSP led to produce grain refined composite that exhibited significant grain refinement, from 41.4±5.9 μm to 1.8±1.9 μm.

ii. The development of basal-dominated texture was evident in the AZ31-nano-CDHA composite as observed from the XRD analysis.
iii. The hardness of the composite was increased due to the smaller grain size and the presence of nano-CDHA.
iv. From the tensile tests data, higher strength (296.3±6.7 MPa) was observed for the composites compared with the base alloy (235±5.5 MPa) without losing the ductility due to the fine grain structure and the incorporated nano-CDHA.
v. Higher cutting forces were recorded for the composite at all the cutting parameters in the drilling operations compared with the base alloy. However, the produced edges of the holes were observed with lower level of material delamination.

REFERENCES

[1] K. K. Chawla, Composite Materials Science and Engineering. 2019 Springer, New York.
[2] G. Uppal, A. Thakur, A. Chauhan, S. Bala, Magnesium based implants for functional bone tissue regeneration – A review. J. Magnes. Alloys **10** (2), 356-386 (2022).
[3] Y. Yang, C. He, E. Dianyu, W. Yang, F. Qi, D. Xie, L. Shen, S. Peng, C. Shuai, Mg bone implant: Features, developments and prospective. Mater. Des. **185**, 108259 (2020).
[4] B. Venkateswarlu, R. Sunil Kumar, B. Ratna Sunil, Magnesium based alloys and composites: Revolutionized biodegradable temporary implants and strategies to enhance their performance. Materialia **27**, 101680 (2023).
[5] K. Kumar, A. Das, S. Bhushan Prasad, Recent developments in biodegradable magnesium matrix composites for orthopaedic applications: A review based on biodegradability, mechanical and biocompatibility perspective. Mater. Today: Proc. **44**, 2038-2042 (2021).
[6] I. Nakahata, Y. Tsutsumi, E. Kobayashi, Mechanical Properties and Corrosion Resistance of Magnesium–Hydroxyapatite Composites Fabricated by Spark Plasma Sintering. Metals **10**, 1314 (2020).
[7] Ehsanollah Moradi, Mehdi Ebrahimian-Hosseinabadi, Mohammad Khodaei, Saeid Toghyani, Magnesium/nano-hydroxyapatite porous biodegradable composite for biomedical applications. Mater. Res. Express **6**, 075408 (2019).
[8] G. Parande, V. Manakari, H. Gupta, M. Gupta, Magnesium-β-Tricalcium Phosphate Composites as a Potential Orthopedic Implant: A Mechanical/Damping/Immersion Perspective. Metals **8**, 343 (2018)
[9] S.Z. Khalajabadi, M.R.A. Kadir, S. Izman, M. Marvibaigi, The effect of MgO on the biodegradation, physical properties and biocompatibility of a Mg/HA/MgO nanocomposite manufactured by powder metallurgy method. J. Alloys Compd. **655**, 266-280 (2016).
[10] Y. Morisada, H. Fujii, T. Nagaoka, M. Fukusumi, MWCNTs/AZ31 surface composites fabricated by friction stir processing. Mater. Sci. Eng. A **419**, 344-348 (2006).
[11] R. Radha, D. Sreekanth, N. Bharti, A. Rana, Mg-1Sn/Al2O3 biodegradable composites: Effect of Al2O3 addition on mechanical, invitro corrosion and bioactivity response. Mater. Res. Express **6** (10), 105411 (2019).
[12] A. Feng, Y. Han, The microstructure, mechanical and corrosion properties of calcium polyphosphate reinforced ZK60A magnesium alloy composites. J. Alloys Compd. **504** (2), 585-593 (2010).
[13] F. Witte, F. Feyerabend, P. Maier, J. Fischer, M. Störmer, C. Blawert, W. Dietzel, N. Hort, Biodegradable magnesium-hydroxyapatite metal matrix composites. Biomater. **28**, 2163-2174 (2007).
[14] M. Razavi, M.H. Fathi, M. Meratian, Microstructure, mechanical properties and bio-corrosion evaluation of biodegradable AZ91-FA nanocomposites for biomedical applications. Mater. Sci. Eng. A **527**, 6938-6944 (2010).
[15] B. Zberg, P.J. Uggowitzer, J.F. Löffler, MgZnCa glasses without clinically observable hydrogen evolution for biodegradable implants. Nat. Mater. **8**, 887-891 (2009).
[16] X.N. Gu, X. Wang, N. Li, L. Li, Y.F. Zheng, X. Miao, Microstructure and characteristics of the metal–ceramic composite (MgCa-HA/TCP) fabricated by liquid metal infiltration. J. Biomed. Mater. Res. B. **99B** (1), 127-134 (2011).
[17] A. Ercetin, D.Y. Pimenov, Microstructure, Mechanical, and Corrosion Behavior of Al_2O_3 Reinforced Mg2Zn Matrix Magnesium Composites. Materials **14** (17), (2021) 4819
[18] Jinlong Su, Jie Teng, Zili Xu, Yuan Li, Corrosion–wear behavior of a biocompatible magnesium matrix composite in simulated body fluid. Friction **10** (1), 31-43 (2022).
[19] K. Kumar, A. Das, S. Bhushan Prasad, Recent developments in biodegradable magnesium matrix composites for orthopaedic applications: A review based on biodegradability, mechanical and biocompatibility perspective. Mater. Today: Proc. **44**, 2038-2042 (2021).
[20] D.G. Filip, V.A. Surdu, A.V. Paduraru, E. Andronescu, Current Development in Biomaterials – Hydroxyapatite and Bioglass for Applications in Biomedical Field: A Review. J. Funct. Biomater. **13**, 248 (2022).
[21] M. Alvarez-Lopez, M.D. Pereda, J.A. Valle, M. Fernandez-Lorenzo, M.C. Garcia-Alonso, O.A. Ruano, M.L. Escudero, Corrosion behaviour of AZ31 magnesium alloy with different grain sizes in simulated biological fluids. Acta Biomater. **6**, 1763-1771 (2010).
[22] M. Bobby Kannan, W. Dietzel, R. Zettler, In vitro degradation behaviour of a friction stir processed magnesium alloy. J. Mater. Sci. Mater. Med. **22**, 2397-2401 (2011).
[23] T. Zhang, W. Wang, J. Liu, L. Wang, Y. Tang, K. Wang, A review on magnesium alloys for biomedical applications. Front. Bioeng. Biotechnol. **10**, 953344 (2022).
[24] G.R. Argade, S.K. Panigrahi, R.S. Mishra, Effects of grain size on the corrosion resistance of wrought magnesium alloys containing neodymium. Corros. Sci. **58**, 145-151 (2012).
[25] G.R. Argade, K. Kandasamy, S.K. Panigrahi, R.S. Mishra, Corrosion behavior of a friction stir processed rare-earth added magnesium alloy. Corros. Sci. **58**, 321-326 (2012).
[26] N.N. Aung, W. Zhou, Effect of grain size and twins on corrosion behaviour of AZ31B magnesium alloy. Corros. Sci. **52**, 589-594 (2010).
[27] H. Wang, Y. Estrin, H. Fu, G.L. Song, Z. Zúberová, The effect of pre-processing and grain structure on the bio-corrosion and

fatigue resistance of magnesium alloy AZ31. Adv. Eng. Mater. **9**, 967-972 (2007).

[28] C. op'tHoog,M. Birbilis, Y. Estrin, Corrosion of pureMg as a function of grain size and processing route. Adv. Eng. Mater. **10** (6), 579-582 (2008).

[29] G.B. Hamu, D. Eliezer, L. Wagner, The relation between severe plastic deformation microstructure and corrosion behavior of AZ31 magnesium alloy. J. Alloys Compd. **468**, 222-229 (2009).

[30] D. Song, A. Ma, J. Jiang, P. Lin, D. Yang, J. Fan, Corrosion behavior of equal-channelangular- pressed pure magnesium in NaCl aqueous solution. Corros. Sci. **52**, 481-490 (2010).

[31] B. Ratna Sunil, T.S. Sampath Kumar, Uday Chakkingal, V. Nandakumar, Mukesh Doble, V. Devi Prasad, M. Raghunath. In vitro and in vivo studies of biodegradable fine grained AZ31 magnesium alloy produced by equal channel angular pressing. Mater. Sci. Eng. C **59**, 356-367 (2016).

[32] R.S. Mishra, P.S. De, N. Kumar, Friction Stir Welding and Processing: Science and Engineering, 2014, Springer, Switzerland.

[33] Amardeep Singh Kang, Ravinder Pal Singh, Sh).ivali Singla, Abhinav Kumar, Friction stir processed magnesium matrix surface composites: a comprehensive review. Funct. Compos. Struct. **6**, 042001 (2024).

[34] B. Ratna Sunil, T.S. Sampath Kumar and Uday Chakkingal Bioactive grain refined magnesium by friction stir processing. Mater. Sci. Forum, **710**, 264-269 (2012).

[35] Xin Wang, Jinlong Su, Cong Li, Jie Tang, Fulin Jiang, Dingfa Fu, Ruichang Du, Jie Teng, Fabrication of high-performance biomedical rare-earth magnesium alloy-based WE43/hydroxyapatite composites through multi-pass friction stir processing. J. Mater. Res. Technol. **33**, 5349-5363 (2024).

[36] Wen Zhang, Jiarui Lu, Lili Tan, Dingrui Ni, Ran Zhang, Qing Zhou, Ke Yang, Qiang Wang, In vitro degradation and in vivo osteogenesis of Mg-Zn-Nd-Zr/HA composites prepared by friction stir processing. J. Magnes. Alloys **12** (12), 4937-4952 (2024).

[37] B. Vandana, P. Syamala, D. Sri Venugopal, S.S.R.K. Imran, B. Venkateswarlu, M. Jagannatham, M. Kolenčík, I. Ramakanth, R. Dumpala, B. Ratna Sunil, Magnesium/fish bone derived hydroxyapatite composites by friction stir processing: studies on mechanical behaviour and corrosion resistance. Bull. Mater. Sci. **42**, 122 (2019).

[38] W. Suchank, M. Yoshimura, Processing and properties of hydroxyapatite-based biomaterials for use as hard tissue replacement implants. J. Mater. Res. **13**, 94-117 (1998).

[39] A. Siddharthan, S.K. Seshadri, T.S. Sampath Kumar, Microwave accelerated synthesis of nanosized calcium deficient hydroxyapatite. J. Mater. Sci: Mater. Med. **15**, 1279-1284 (2004).

[40] M.K. Elipey, P.S. Kishore, B. Ratna Sunil, AZ31-calcium-deficient hydroxyapatite (CDHA) composites produced by friction stir processing: controlling the degradation by enhancing the biomineralisation. Can. Metall. Q. 1-12. (2024) 10.1080/00084433.2024.2351346

[41] G.V.V. Surya Kiran, K. Hari Krishna, Sk. Sameer, M. Bhargavi, B. Santosh Kumar, G. Mohana Rao, Y. Naidubabu, R. Dumpala, B. Ratna Sunil, Machining characteristics of fine grained AZ91 Mg alloy produced by friction stir processing. Trans. Nonferrous. Met. Soc. China **27**, 804 (2017).

[42] P. Hemendra, R. Dumpala, B. Ratna Sunil, Machining characteristics and corrosion behaviour of grain refined AZ91 Mg alloy produced by friction stir processing: Role of tool pin profile. Trans. Ind. Inst. Met. **71** (4) 951-959 (2018).

[43] M. Venkataiah, T. Anup Kumar, K. Venkata Rao, S. Anand Kumar, I. Siva, B. Ratna Sunil, Effect of grain refinement on corrosion rate, mechanical and machining behaviour of friction stir processed ZE41 Mg alloy. Trans. Ind. Inst. Met. **72**, 123-132 (2019).

[44] N. Saikrishna, G.P.K. Reddy, M. Balakrishnan, B. Ratna Sunil, Influence of bimodal grain size distribution on the corrosion behaviour of friction stir processed biodegradable AZ31 magnesium alloy. J. Magnes. Alloys **4**, 68-76 (2016).

[45] ASTM Standard E112-12. Standard test methods for determining average grain size, (2012) ASTM International, West Conshohocken, PA, DOI: 10.1520/E0112-12.

[46] ASTM Standard E8/E8M-11, Standard Test Methods for Tension Testing of Metallic Materials, (2009) ASTM International, West Conshohocken, PA.
DOI: https://doi.org/10.1520/E0008_E0008M-22